



CHALMERS
UNIVERSITY OF TECHNOLOGY

Assessing the Multi-Regime Capability of the Super-Grid Linear Eddy Model (SG-LEM) Using the Darmstadt Multi-Regime Burner

Downloaded from: <https://research.chalmers.se>, 2025-04-10 13:35 UTC

Citation for the original published paper (version of record):

Murlidharan Menon, A., Kerstein, A., Oevermann, M. (2025). Assessing the Multi-Regime Capability of the Super-Grid Linear Eddy Model (SG-LEM) Using the Darmstadt Multi-Regime Burner. *Flow, Turbulence and Combustion*, 114(2): 395-420.
<http://dx.doi.org/10.1007/s10494-024-00602-x>

N.B. When citing this work, cite the original published paper.



Assessing the Multi-Regime Capability of the Super-Grid Linear Eddy Model (SG-LEM) Using the Darmstadt Multi-Regime Burner

Abhilash Menon¹ · Alan Kerstein² · Michael Oevermann^{1,3}

Received: 3 July 2024 / Accepted: 25 October 2024 / Published online: 29 November 2024
© The Author(s) 2024

Abstract

Recent advances in combustion modelling for Large Eddy Simulation (LES) have increasingly utilised lower-dimensional manifolds, such as Flamelet Generated Manifolds and Flamelet/Progress Variable methods, due to their computational efficiency. These methods typically rely on one-dimensional representations of flame structures, often assuming premixed or non-premixed configurations. However, practical combustion devices frequently operate under partially-premixed conditions and present challenges due to mixture inhomogeneities and complex flow features. The Linear Eddy Model (LEM) offers an alternative by directly simulating turbulence-chemistry interactions without presuming specific flame structures. However, traditional LES-LEM approaches are computationally quite expensive due to the need for resolved LEM domains to be embedded in every LES cell. The authors developed the Super-Grid LEM (SG-LEM) method (Comb. Theor. Model. 28, 2024) to address these computational challenges by coarse-graining the LES mesh and embedding individual LEM domains within *clusters* of LES cells. This study evaluates SG-LEM in the context of the Multi-Regime Burner (MRB) introduced by Butz et al. (Combust. Flame, 210, 2019), which features both premixed and non-premixed flame characteristics. SG-LEM simulations of the MRB case demonstrate the method's sensitivity to clustering parameters, with flow-aligned clusters significantly improving flame stability. LEM domains on the super-grid were able to represent the MRB flame topology while LES radial profiles including velocity, mixture fraction, temperature, and CO mass fraction, were validated against experimental data and also reference simulations using standard combustion closures. The work also investigates discrepancies in CO profiles using conditional statistics and stand-alone LEM simulations. Finally, the work identifies areas of improvement for the SG-LEM framework, in particular relating to cluster generation, and (advective and diffusive) mass exchange between neighbouring LEM domains, as well as possible solutions for future SG-LEM implementations which could improve the model's predictive capability.

Keywords LES · Linear Eddy Model · Multi-regime combustion · Partially premixed flames

1 Introduction

In recent years, researchers have increasingly turned to lower-dimensional manifolds for combustion closure in large eddy simulation (LES). This choice stems from their superior computational efficiency in advancing overall chemistry compared to reaction-rate closures. These manifolds are typically one-dimensional (1D) representations of fundamental flame structures. They underpin techniques like flamelet generated manifolds (FGM) and flamelet/progress variable (FPV) approaches. The canonical flame configurations considered are often counter-flow diffusion type or freely-propagating (premixed) flames, as utilised in the FPV method. As a result, flame structures are described as functions of few fundamental independent variables such as mixture fraction and reaction progress variable, in addition to parameterise variables, e.g., scalar dissipation rate, to account for non-equilibrium effects. In general, only laminar flame structures are considered and turbulence-chemistry interaction (TCI) is taken into account parametrically.

Applying manifold techniques to reactive LES usually involves assuming a specific flame structure, either premixed or non-premixed. However, practical combustion devices like internal combustion engines (ICEs) and gas turbines often operate under partially-premixed conditions, exhibiting mixture inhomogeneities and intricate flame structures that display attributes of both premixed and non-premixed combustion. While these inhomogeneities might be deliberately introduced to enhance flame stability or combustion efficiency, they introduce modelling complexities due to the coexistence and interaction of the two conditions. In this study, we adopt the term ‘multi-regime’,¹ consistent with the referenced literature, to describe such flame structures.

The Linear Eddy Model (LEM) stands out as another form of a lower-dimensional manifold. Unlike FPV/FGM, LEM doesn’t rely on presumptions about a premixed or non-premixed flame structure. In the LEM approach, the combined reaction-diffusion-stirring equations are evolved across a fully resolved 1D domain. In this context, the influence of small-scale (turbulent) stirring is conceptualised through a sequence of length-scale breakdowns in scalar profiles via a series of rearrangement events called ‘triplet maps’. This is to say that TCI is directly simulated in the model and not treated parametrically.

The conventional utilisation of LEM as a combustion closure for turbulent combustion in LES, usually called LES-LEM (Smith and Menon 1998; Arshad 2019), necessitates significant computational resources because a unique, highly resolved, LEM domain is advanced for each LES cell concurrently with the flow solver. Between successive LES advancements, LES-resolved large-scale advection is captured by means of Lagrangian transport of LEM domain fragments between neighbouring LEM domains, a procedure known as ‘splicing’; this also contributes to the computational workload. To achieve substantial speed-up, an approach involving coarse-graining of the LES mesh has been developed. Here, an individual LEM domain is encapsulated within a cluster of LES cells. This approach, known as the ‘super-grid’-LEM or SG-LEM, was introduced in Menon et al. (2024) and validated for a premixed ethylene-air flame. Figure 1 compares traditional LES-LEM with the SG-LEM closure method.

Other studies have used coarsening to address the costs associated with traditional LES-LEM closure, e.g., the dual-grid approach by Ranjan et al. (2016) in which LEM profiles

¹ Note that some authors use the term ‘mode’ to differentiate premixed and non-premixed flames, and ‘regime’ to describe non-equilibrium effects, e.g., flamelet-regime.

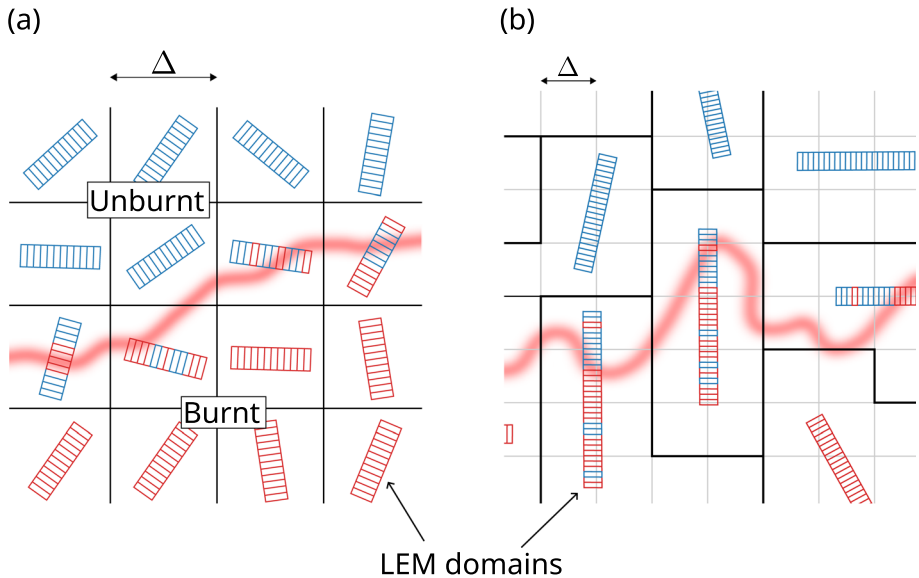


Fig. 1 Comparison of **a** LES-LEM, and **b** SG-LEM where the thick lines indicate the cell agglomerations or clusters. Δ is the LES cell size

for coarse mesh cells are re-constructed every time step using LES-resolved scalar gradients instead of splicing. Also notable is the use of Adaptive Mesh Refinement (AMR) by Maxwell et al. (2015) for their compressible LEM formulation (C-LEM) which was demonstrated for 1D flames with prescribed turbulent production, including flame/shock interactions.

LEM's (and by extension, SG-LEM's) mode- and regime-independent nature potentially makes it a suitable technique for the numerical study of multi-regime flames with differing levels of turbulence within one flame.

2 Multi-Regime Burner (MRB)

This work focuses on the numerical study of the Darmstadt Multi-Regime Burner (MRB) test case, as presented by Butz et al. (2019, 2022). The burner head is shown schematically in Fig. 2. It uses three gas streams marked as 'Jet', 'Slot 1' and 'Slot 2' along with a co-flow. The equivalence ratios (ϕ) and jet velocities (u) shown in Fig. 2 correspond to the operating point 'MRB26b'. This condition for the burner head is characterised by a premixed flame from the annular jet emerging from Slot 2 that is stabilised behind the conical bluff body, while the high equivalence ratio for the central jet results in a lifted diffusion flame. This inner flame exhibits complex multi-regime combustion patterns (Butz et al. 2019). The experimental data-set provides well-defined boundary and inflow conditions for a multi-regime methane-air flame along with detailed results for mean velocity, temperature and select species; as well as their fluctuations. Butz et al. (2019) also present a prior analysis on the use of tabulated closure, using both premixed and non-premixed flamelets, for this case, which showed promising results but also some potential inaccuracies in CO mass fractions.

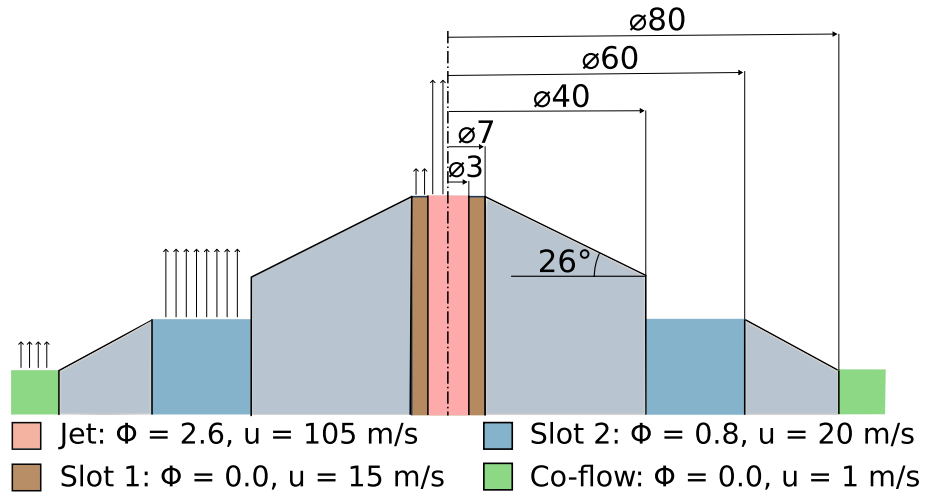


Fig. 2 Schematic of the Darmstadt multi-regime burner (MRB)

The main objective of this work is to further evaluate the predictive capabilities of this relatively new combustion closure, SG-LEM, in a novel and challenging (experimental) flame setup. We compare time averaged simulation data with experimental values, and also with standard combustion models. Special attention is given to CO due to potential inaccuracies mentioned previously, which are also corroborated by a recent LES study by Popp et al. (2021). The flame does not exhibit strongly transient behaviour (i.e., extinction, reignition and auto-ignition) which justified the use of tabulated flamelets (Popp et al. 2021; Engelmann et al. 2023; Zhang et al. 2023). The statistical stationarity also lends itself to SG-LEM as the model uses “on-the-fly” tabulation that is continually updated over time and is tailored to the case being simulated. LEM domains, as will be discussed, can fully resolve flame structures in one dimension, which could be beneficial for challenging diagnostics like CO.

3 The Linear Eddy Model

3.1 Overview

LEM has unique advantages compared to other lower dimensional manifolds, other than the aforementioned regime independence. It advances species and thermal diffusion in physical, albeit 1D, space. This representation enables full resolution of the turbulent flame structure. In the LES, closures for velocity, concentrations and energy are eddy diffusive, hence combining diffusional and advective effects. In LES-LEM, LEM domains simulate advection and diffusional effects below the LES filter width (or LES cells size for implicit LES). LEM domains advance chemistry because LES eddy-diffusivity SGS closure does not adequately capture TCI.

3.2 Reaction-Diffusion Advancement

Equations for the conservation of energy and species mass fraction are time advanced along the LEM domain y as

$$\rho c_p \frac{\partial T}{\partial t} = -\frac{\partial Q}{\partial y} + S_T, \quad (1)$$

and

$$\rho \frac{\partial Y_\alpha}{\partial t} = -\frac{\partial j_\alpha}{\partial y} + S_\alpha, \quad (2)$$

where T , ρ , C_p and Y_α represent the temperature, density, specific heat capacity and mass fraction of species α , respectively. The fluxes Q and $j_{\alpha,x}$ are due to thermal and species diffusion while source terms S_T and S_α represent the effect of chemical reactions that are evolved individually in the ‘wafers’ comprising the discrete domain. Species (i.e. Fickian) fluxes are computed from concentration gradients, i.e., $j_\alpha = -D_\alpha \frac{\partial Y_\alpha}{\partial y}$ where diffusivities D_α are determined from

$$D_\alpha = \frac{\kappa}{Le \rho c_p}, \quad (3)$$

where κ is the thermal conductivity, c_p is the specific heat at constant pressure, and Lewis number Le is set to unity. A similar gradient approach is also used for thermal (i.e. Fourier) flux. Species-dependent Le can be and has been implemented in LEM such that differential-diffusion effects are captured, as demonstrated by Kerstein et al. (1995). In this work, however, the choice of operator splitting (explained in the upcoming Sect. 4.1) is a sufficient departure from time-accurate advancement that species-dependent Le would not improve fidelity.

Dilatation is modelled by applying an expansion ratio to each wafer as a function of the instantaneous density relative to the density at the previous time instance i.e.,

$$\Delta y_i^{\text{new}} = \Delta y_i \left(\frac{\rho_i}{\rho_i^{\text{new}}} \right), \quad (4)$$

Δy_i being the size of wafer i . For further details we refer to Sec. 2.3 of Menon et al. (2024).

3.3 Small-Scale Stirring

Turbulent stirring is simulated using physics-based breakdowns of scalar spatial structures induced by spatial rearrangements within the LEM domains called ‘triplet maps’. Each rearrangement, or ‘eddy-event’, simulates the effect of a single eddy turnover on all scalar fields within the mapped interval. Eddy-events interrupt the advancement of Eqs. (1) and (2), which is to say the time, or *epoch*, is the third parameter for a triplet map. The frequency of eddy-events simulates the intensity of small-scale stirring. The eddy location y_0 is sampled from a uniform distribution in $[0, l_{\text{LEM}}]$ with l_{LEM} being the length of the LEM domain. This is to say that an eddy is equally likely at any point the LEM domain. The extent l , however, is sampled from the frequency distribution

$$f(l) = \frac{5}{3} \frac{l^{-8/3}}{\eta^{-5/3} - l_t^{-5/3}}, \quad (5)$$

where η is the Kolmogorov dissipative scale and l_t is the integral length scale. In traditional LES-LEM, l_t is set the LES cell sizes, effectively LEM resolves flame structures between LES cell size and the dissipative scales. As for the epoch, eddy-events are implemented as a Poisson process in time with a mean equal to $\lambda \times l_{\text{LEM}}$ where the eddy-frequency, λ , is given by

$$\lambda = \frac{54}{5} \frac{\nu Re_t [(l_t/\eta)^{5/3} - 1]}{C_\lambda l_t^3 [1 - (\eta/l_t)^{4/3}]}. \quad (6)$$

Here, Re_t is the turbulent Reynolds number. For a given turbulence intensity, the Kolmogorov scale is approximated as

$$\eta = N_\eta l_t Re_t^{-3/4}. \quad (7)$$

The model constants C_λ and N_η can be tuned to control the eddy-sampling-rate and eddy-size distribution, respectively. The reader is referred to Kerstein (1991) for more details on triplet mapping.

3.4 Large Scale Advection

As mentioned before, in LES-LEM large scale advection is modelled in LEM by Lagrangian transport of LEM domain fragments² between neighbouring domains in a process known as ‘splicing’. Previous LES-LEM studies use the ratio of volumetric flux to control volume (size) to determine the fragment mass (Arshad et al. 2018; Sankaran 2003), i.e.,

$$m_{\text{frag}} = \frac{\phi \Delta T_{\text{LES}}}{V_{\text{cell}}} m_{\text{LEM}}, \quad (8)$$

where m_{frag} is the mass of the LEM fragment to be exchanged between domains, m_{LEM} is the total mass on the donor LEM domain, $\phi = \vec{u} \cdot \vec{A}$ is the volumetric flux through a face of area A (between donor and receiver LES cells) during interval ΔT_{LES} , and V_{cell} is the volume of the donor LES cell. Advection in three dimensions is carried out using several 1D splicing operations. For a hexahedral LES cell, a splicing operation could, e.g., consist of three attachment and three detachment operations involving the six faces of the LES cell. This was extended to unstructured meshes by Arshad et al. (2018), where cells can be tetrahedral or polyhedral.

3.5 Coupling Between LEM and LES

In standard LES-LEM an LEM domain is embedded in each LES cell and the local (filtered) thermochemical state is set to the local Favre- or conventionally-averaged LEM state for any given scalar ψ as

² Here, a ‘fragment’ is defined as a contiguous interval in the LEM coordinate y .

$$\tilde{\psi} = \frac{\sum_{i=0}^N \rho_i \psi_i}{\sum_{i=0}^N \rho_i}, \quad (9)$$

where N denotes the total number of wafers of the embedded LEM domain.

4 Super-Grid LEM (SG-LEM)

4.1 Chemistry Closure of LES Using LEM

LES-LEM places tremendous demand on compute resources compared to standard methods, even reaction-rate closures, simply due to the fact that each wafer of the embedded LEM domains requires reaction advancement. For reaction-rate closures, chemistry advancement is usually the most demanding sub-step in reactive simulations and for LES-LEM this expense scales with the LEM domain resolution. Splicing is an additional computational effort which scales with the number of LEM domains. Although the method can capture thin flame-fronts on a sub-grid level, it is usually limited to simple global chemical mechanisms and low Reynolds number (Re) applications. More recent studies, however, employ LES-LEM closure with reduced and skeletal mechanisms, e.g., Li et al. (2018, 2016), due to improvements in computational capabilities. Grøvdal (2018) shows that the compute-time for LEM scales with $Re^{3/4}$. Chemical source terms in Eqs. (1) and (2) usually require a stiff numerical integrator, e.g., CVODE (Hindmarsh et al. 2005) which is used in this work. A triplet map, as mentioned before, requires an interruption to the above time-advancements which, in practice, entails a start-restart cycle of the numerical integrator. It's easily inferred that frequent interruptions produce a significant computational overhead, in particular with high order multi-step methods such as BDF (backward differentiation formula).

The operator splitting used for LEM advancement has a large impact on this overhead. For a formally second order Strang-splitting approach, each eddy is implemented at its precise epoch, which means reaction-diffusion advancement is to be carried out between successive eddy-events. Therefore, high Re (or high λ) cases can become costly to compute due to the high frequency of interruptions. An alternative 'blocked-sequence' operator splitting (Menon et al. 2024) can be used where all eddy-events within an LES time-step are implemented sequentially at once, followed by reaction-diffusion advancement for the whole LES time-step. Poisson processes determine the number of eddy-events for the given time step. This approach significantly reduces the number of start-restart cycles for high Re scenarios.

Computational speed-up was the major motivation behind the development of SG-LEM (Menon et al. 2024). Significant performance improvement was achieved by using coarse-graining of the LES mesh. This results in a down-scaling of the total number of LEM domains (and therefore wafers) that need to be time-advanced. In SG-LEM, triplet maps represent all scales of advection below the cluster scale, encompassing both the subgrid and some of the resolved scales of the LES. Splicing represents advection at the cluster and larger scales. Thus, the model has two parallel representations, LES and SG-LEM, of all scales of diffusion and advection, where only SG-LEM advances chemistry. Coupling between the LEM domains and the LES solution is performed at the cluster level, and requires some means of obtaining LES-resolved data from the embedded LEM domain, as opposed to Eq. (9) which can only report data at SG resolution. It is,

however, a useful secondary output of the model where cluster-level fields are set to the Favre-mean of the fields over the corresponding LEM domains, i.e., using Eq. (9).

The coupling scheme used in this work is adapted from RILEM (Representative Interactive Liner Eddy Model) closure (Doubiani et al. 2024; Lackmann et al. 2018), and is described as follows. LES coupling here is achieved using a presumed PDF approach similar to FGM/FPV, where the first moment of the weighted PDF provides the local LES chemical state. This can be written as

$$\tilde{\psi}_{LES} = \int_0^1 \langle \psi_{LEM} | Z, c \rangle P(Z, c) dZ d. \quad (10)$$

Assuming statistical independence of Z and c gives

$$\tilde{\psi}_{LES} = \int_0^1 \langle \psi_{LEM} | Z, c \rangle P(Z)P(c) dZ dc. \quad (11)$$

The current framework was built with the flexibility of PDF choices in mind; hence, it can be extended to a joint PDF using, e.g., the copula method by Darbyshire and Swaminathan (2012), which does not require the assumption of statistical independence. For this MRB case, however, the choice of independent Z and c is consistent with previous studies, e.g., Zhang et al. (2023), who utilised presumed PDFs with tabulated chemistry to reproduce accurate scalar fields.

The LEM domain provides conditionally binned statistics $\langle \psi | Z, c \rangle$ relevant to its cluster with the solution space defined by mixture fraction Z and progress variable c as independent variables. Each LEM is informed by local turbulence level via Re_t , and also large-scale advection via splicing. Implementation-wise, each cluster is associated with an individual solution table that is updated by LEM advancement. The ‘persistence’ method from Menon et al. (2024) was used to obtain the state-space-averaged solution tables, where each bin value is retained until the appropriate Z - c combination is detected on the LEM domain. This continually updates the solution table and retains statistical fidelity despite the small number of LEM wafers at any given instant. The presumed PDF approach requires the LES advancement of the filtered mean mixture fraction and mean and progress variable i.e., \tilde{Z} and \tilde{c} as:

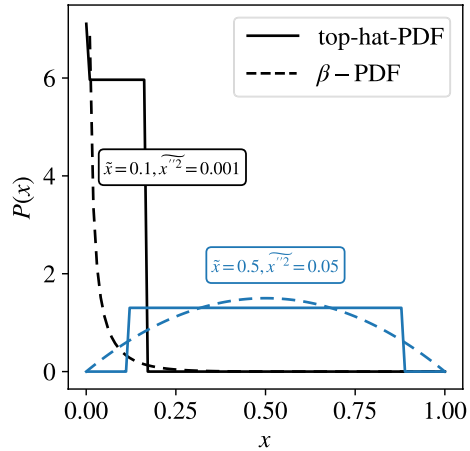
$$\frac{\partial(\bar{\rho}\tilde{Z})}{\partial t} + \frac{\partial}{\partial x_j}(\bar{\rho}\tilde{u}_j\tilde{Z}) = \frac{\partial}{\partial x_j} \left(-\frac{\mu_t}{Sc_t} \frac{\partial \tilde{Z}}{\partial x_j} \right) + \dot{m}_{\text{evap}} \quad (12)$$

and

$$\frac{\partial(\bar{\rho}\tilde{c})}{\partial t} + \frac{\partial}{\partial x_j}(\bar{\rho}\tilde{u}_j\tilde{c}) = \frac{\partial}{\partial x_j} \left(-\frac{\mu_t}{Sc_t} \frac{\partial \tilde{c}}{\partial x_j} \right) + \bar{p}\tilde{c}. \quad (13)$$

Here, μ_t is turbulent viscosity, Sc_t the turbulent Schmidt number, \dot{m}_{evap} denotes a fuel source (e.g. a spray model, not used in this case) and \tilde{c} is the chemical source term. In this work, the ‘extended top-hat’ PDF of Floyd et al. (2009) is assumed for Z , and Dirac δ -peaks are assumed for c . It is able to handle a wide range of scalar variances and is more efficient to compute than β -PDFs that are typically used for mixture fraction. This formulation also incorporates weighted δ -peaks to generate PDF shapes near the end ranges, i.e., for mean values near 0 and 1. Figure 3 plots two examples of top-hat PDF shapes.

Fig. 3 Top-hat PDF shapes for a random variable x . β -PDF shapes, typically used for Z , are shown for comparison. Computed using mean \bar{x} and variance $\overline{x''^2}$ in the boxes



Scalar variance $\overline{Z''^2}$ is computed using an algebraic model from Pierce and Moin (1998) as

$$\overline{Z''^2} = C_v \Delta^2 |\nabla \tilde{Z}|^2, \tag{14}$$

where C_v is a model constant set to 1/12.

For LEM domains, Z for each wafer is computed using elemental mass fractions of C, H, O and N - along the lines of Bilger (1977). The local Z -value is then used to determine the correct Z -bin of the solution table. Reaction progress c is computed as

$$c = \frac{Y_c - Y_{c,u}}{Y_{c,b} - Y_{c,u}}, \tag{15}$$

where

$$Y_c = Y_{CO_2} + Y_{H_2O}, \tag{16}$$

and subscripts ‘b’ and ‘u’ correspond to burnt and unburnt values. The unburnt value is determined from the local Z , while the burnt value is set to the equilibrium state of the corresponding Z -bin, both of which are pre-computed using a constant enthalpy assumption.

4.2 Splicing for SG-LEM

The splicing routine for LES-LEM (cf. Sect. 3.4) is modified for the super-grid variant in the following ways. First, as each LEM domain is embedded in a cluster of LES cells, aggregate fluxes i.e., fluxes across cluster faces, are used to compute splicing fractions. Effectively, fluxes are *super-grid-resolved*. Second, as neighbouring clusters can feature large differences in their volumes, LEM fragments are compressed or expanded based on a nominal cross section Γ , defined as

$$\Gamma = V_c / l_t. \tag{17}$$

For this purpose, a *length-based* splicing scheme was selected in contrast to the *mass-based* routine of LES-LEM, cf. Eq. (8). This is written as

$$l_{\text{frag}} = \frac{\phi \Delta T_{\text{LES}}}{V_{\text{SG}}} l_{\text{LEM}}. \quad (18)$$

Fragment lengths are then modified to effect the aforementioned expansion (or contraction) when splicing between clusters of differing volumes, i.e.,

$$l_{\text{frag}} := l_{\text{frag}} \frac{\Gamma_{\text{recv}}}{\Gamma_{\text{don}}}, \quad (19)$$

where Γ_{recv} and Γ_{don} are the nominal cross-sections of the receiver and donor LEM domains. Note that the above is applied on a per wafer basis for the fragment and conserves mass, temperature as well as composition. The ‘flux-ordered’ ordering scheme of Arshad (2019) is used in this work. Here, attachments are ordered in ascending order of flux through the associated face whereas detachments are ordered in descending order of flux. This way, higher fluxes translate to larger displacements (in physical space) of LEM fragments.

The implementation details of the splicing algorithm are omitted here for brevity but can be found in Sec. 2.6 of Menon et al. (2024).

5 LES-SG-LEM Modelling Approach

5.1 LES Formulation

The Favre-filtered LES balance equations for mass, momentum, and total enthalpy are given as:

$$\frac{\partial \bar{\rho}}{\partial t} + \frac{\partial \bar{\rho} \tilde{u}_i}{\partial x_i} = 0, \quad (20)$$

$$\frac{\partial \bar{\rho} \tilde{u}_i}{\partial t} + \frac{\partial \bar{\rho} \tilde{u}_i \tilde{u}_j}{\partial x_j} = -\frac{\partial \bar{p}}{\partial x_i} + \frac{\partial}{\partial x_j} \left(\bar{\tau}_{ji} + \bar{\tau}_{ji}^{\text{sgs}} \right), \quad (21)$$

and

$$\frac{\partial (\bar{\rho} \tilde{h})}{\partial t} + \frac{\partial \bar{\rho} \tilde{u}_j \tilde{h}}{\partial x_j} = \tilde{u}_j \frac{\partial \bar{p}}{\partial x_j} + \frac{\partial}{\partial x_j} \left(-\alpha_{\text{Eff}} \frac{\partial \tilde{h}}{\partial x_j} \right) + \frac{\partial p}{\partial t}. \quad (22)$$

where the operators $\overline{(\cdot)}$ and $\tilde{(\cdot)}$ represent conventional and Favre filtering operations, respectively. Symbols ρ , u , p and h respectively denote density, velocity, pressure, and enthalpy of the fluid. The terms $\tilde{u}_j \partial \bar{p} / \partial x_j$ and $\partial p / \partial t$ are set to zero for low-Mach-number open flames, as is the case here. Sutherland’s law (Sutherland 1893) is used to compute temperature dependent viscosity. Typically, gradient assumption would be used for turbulent flux $\bar{\tau}_{ji}^{\text{sgs}}$. Here we employ the Smagorinsky subgrid model (Smagorinsky 1963) for the turbulent momentum fluxes, whereas the subgrid turbulent flux for species mass fraction is implicit within mapping of LEM-derived mass fractions using Eqs 10 and (13). The above equations are complemented by the caloric equation of state

$$h = \int_0^T c_p(\theta) d\theta, \quad (23)$$

specific heat is approximated using the polynomial expression

$$c_{p,\alpha}(\theta) = \sum_{k=0}^4 c_{k,\alpha} \theta^k \quad (24)$$

and composition data, i.e.,

$$c_p(\theta) = \sum_{\alpha=1}^N Y_{\alpha} c_{p,\alpha}(\theta). \quad (25)$$

Here, $c_{k,\alpha}$ are the NASA polynomial coefficients (McBride et al. 2002) which are known and tabulated. This simplifies the integral in Eq. (23) to

$$h(T) = \sum_{\alpha=1}^N \sum_{k=0}^4 \frac{c_{k,\alpha}}{k+1} T^{k+1} + c_{5,\alpha}. \quad (26)$$

Using \tilde{h} , the LES temperature \tilde{T} can be obtained as a Newton-Raphson iterative solution to the expression

$$T := T - \frac{h(T) - \tilde{h}}{dh/dT} \quad (27)$$

with dh/dT set to $c_p(T)$ using Eq. (25), and an initial guess for T .

5.2 LES Setup

An LES-SG-LEM solver was implemented in OpenFOAM v. 9 (Jasak 1996) using the low-Mach-number formulation for the LES equations. Pressure and velocity equations are advanced using the PISO (pressure-implicit splitting of operators) algorithm of Issa et al. (1986). The LES mesh here is cylindrical with a radius 200 mm and an axial length of 183 mm consisting of hexahedral cells with sizes ranging from 0.1 to 0.4 mm, see Fig. 4. A second order backward implicit temporal scheme together with second order spatial discretization are employed. Time-resolved inlet velocities for the jet and Slot 2 are obtained from precursor LES simulations for a pipe-cyclic and an annular-cyclic setup from which fully developed turbulent data were obtained for the appropriate bulk velocities. A laminar velocity profile was used for Slot 1. The boundary conditions for \tilde{Z} for the jet and Slot 2 are 0.131 and 0.044, respectively, corresponding to the ϕ values in Fig. 2. For Slot 1 and the co-flow, $\tilde{Z} = 0$.

5.3 Super-Grid Setup

Coarse-graining of the LES mesh is handled by the MGRIDGEN library (Moulitsas and Karypis 2001), which performs the clustering independently in each processor domain. Even though processor decomposition and mesh agglomeration are different steps, the latter is not independent of the former – cluster shapes produced by MGRIDGEN are

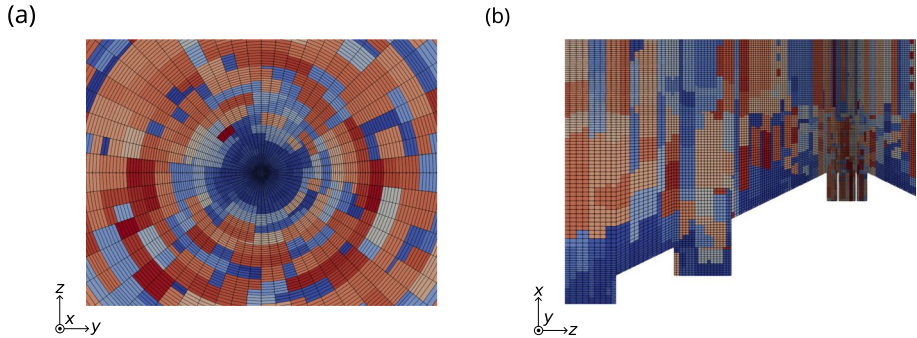


Fig. 4 Zoomed-in view of clustering near **a** the outlet face, and **b** the burner wall. Black lines indicate LES cells and colours are indicative of clusters

influenced by shapes of the individual processor domains. It is also agnostic of boundary conditions or any prescribed physical criteria, typical of such automated procedures. MGRIDGEN tries to minimise the (weighted-average) aspect ratio of clusters, using cluster sizes as the sole provided input.

Large-scale transport (splicing) plays an important role in flame stability. Driven by SG-resolved fluxes, it is heavily influenced by the sizes and shapes of the clusters, cf. Fig. 2. Initial tests using standard decomposition routines such as ‘scotch’ (Pellegrini and Roman 1996) and ‘hierarchical’ produced unphysical flame quenching and did not lead to a stable flame. The domain shapes created by the above routines led to clusters that were not flow-aligned, which led to inaccuracies in splicing transport and the aforementioned quenching. In particular, this was observed for the outer flame, downstream of Slot 2, where excessive (inaccurate) transport of fresh charge, radially, into the flame front near the recirculation zone led to cooling of the burnt products. In general, a stationary flame-front requires a balance between the turbulent flame speed and velocity of fresh charge normal to the flame front. The excessive splicing transport of fresh charge violates this condition. The quenched outer flame in turn, could no longer support the inner flame.

This problem was mitigated by exercising indirect control over the cluster shapes by leveraging the dependence of clustering outcome on processor decomposition. A ‘structured’ decomposition was performed, where a two-dimensional decomposition was first performed on the outlet face using the scotch method, and subsequently projected in the axial (x) direction. These were performed using OpenFOAM’s `decomposePar` utility to produce 256 processor domains. Additionally, accurate fuel-air distribution is necessary to obtain the correct lift-off behaviour of the central flame. This is also promoted by controlling the cluster shapes. A cluster size of 64 was found to provide a good balance between accuracy of large-scale transport and simulation time. The decomposition and agglomeration parameters, together, give flow-aligned clusters as shown in Fig. 4. This method of indirect cluster shape control may not be suited for more complex geometries and is seen as an intermediate solution given the limitations of the current SG-LEM framework. A future improvement will be the use of a simple closure to run an inexpensive pre-simulation that approximates the flow field for clustering purposes, then run SG-LEM for chemical detail using the chosen cluster partitioning.

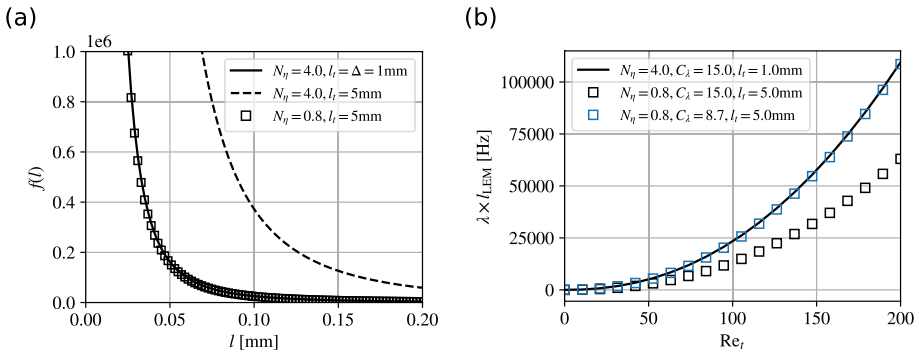


Fig. 5 The effect of LEM constants. Panel **a** shows the effect of N_η on eddy size distribution using $Re_t = 100$ and $C_\lambda = 15.0$. Panel **b** the effect of N_η and C_λ on eddy frequency

5.4 LEM Setup

The LEM grid resolution was set to $100\ \mu\text{m}$, which enabled reasonable simulation times. This resolution was also motivated by Engelmann et al. (2023), who utilised an LES mesh of the same equidistant grid spacing to simulate the MRB case. Additionally, the study did not employ artificial thickening of the flame front, presumed PDFs, or a turbulence model, and also determined the impact of the under-resolved scales as being negligible using sub-grid variance of the progress variable, i.e., the resolution of $100\ \mu\text{m}$ was deemed sufficient to resolve TCI. A skeletal mechanism for lean CH_4 from Sankaran et al. (2007) with 17 species and 73 reactions was used for evaluating reaction rates, enthalpies and transport coefficients. LEM advancement was carried out using the blocked-sequence operator splitting discussed previously. Although this introduces a splitting bias, stand-alone LEM simulations using domain sizes and turbulence intensities that are expected for this test case revealed negligible differences in the solution tables, particularly when time steps typical of LES were used.

Previous LES-LEM studies have used LEM parameter values of $C_\lambda = 15$ based on 1D simulation of freely propagating flames (Smith and Menon 1997) and $N_\eta = 4$ (Arshad 2019; Menon and Calhoun 1996; Calhoun and Menon 1996). However, in the case of SG-LEM we assumed $l_t = 0.5 L_{\text{LEM}}$ in Eqs. (5) and (6), where the domain lengths are set using the aggregated cell volumes as

$$L_{\text{LEM}} = V_C^{1/3}, \tag{28}$$

where V_C is the volume of the cluster. N_η and C_λ can then be related to their literature values as follows: if we assume that the SG-LEM domains correspond to their LES counterparts as $l_t^{\text{SG}} = 5 l_t^{\text{LES}}$, the Kolmogorov scale estimate using Eq. (7) would require $N_\eta = 0.8$ to reflect a similar size distribution given by Eq. (6), shown in Fig. 5 a. Then, in order to obtain a similar eddy-sampling-rate, C_λ must be set to to 8.707, as shown in Fig 5b. Hence, the LEM constants are set to $N_\eta = 0.8$ and $C_\lambda = 8.707$ for this study. The ratio of LEM domain lengths and LES cell sizes was determined by visual inspection of the mesh and the super-grid. Since the two LEM parameters are tuned independently, a single ratio of 5 was chosen for simplicity despite the radial mesh and super-grid. Finally, Re_t is computed for each cluster using the volume averaged turbulent kinetic subgrid energy k^{sgs} , i.e.,

$$k_C = \frac{\sum_i^N k_i^{\text{sgs}} V_i}{V_C}, \quad (29)$$

$$Re_i = \frac{\sqrt{\frac{2}{3}} k_C L_{\text{LEM}}}{\nu_{\text{LEM}}}, \quad (30)$$

where i is the LES index of a cluster comprising N cells, and ν_{LEM} is the average kinematic viscosity on the corresponding LEM domain.

LEM evolved scalars, in particular Y_α and \dot{c} , are binned into 150×100 equally spaced bins corresponding to Z - and c -space providing the conditional terms (solution tables) $\langle \psi | Z, c \rangle$ in Eq. 10. While the range of $c \in [0, 1]$ is fully populated, a reduced Z -space with $Z \in [0, 0.15]$ has been used for better resolution. The reduced Z -space reflects the expected limits of \tilde{Z} in the domain during the simulation, with the added benefit of reducing memory usage.

6 Results

This section analyzes the simulation results using instantaneous snapshots followed by comparison of time-averaged scalar profiles profiles with experimental data as well as reference simulations using established combustion models. Finally, conditional statistics for CO are analysed for the inner and outer flames.

6.1 Instantaneous Fields and Flame Topology

The MRB simulation required approximately 30,000 core-hours to simulate 0.06 s of time, with data collected for time averaging over 0.03 s. In this section, we present instantaneous solution fields, including results from the SG-LEM mapping closure. All LES-resolved fields except velocity and mixture fraction are obtained using the mapping closure. The secondary model output (cf. Sect. 4.1) is also reported at SG resolution. This is termed ‘LEM-level’ henceforth, and marked simply as ‘LEM’ in the figures. This is followed by comparisons of time-averaged data with experimental measurements, including conditional statistics for CO. Figure 6a displays an instantaneous velocity plot with streamlines that represent the time-averaged velocity clearly showing the strong re-circulation zone downstream. Figure 6b depicts mixture fraction, at LES-resolution \tilde{Z} (left half) and the LEM-level \tilde{Z}_{LEM} (right half). \tilde{Z}_{LEM} reflects splicing (driven by SG-resolved fluxes), with turbulent stirring playing a secondary role. \tilde{Z} , however, results from advancement of Eq. (12). The similarity in instantaneous structures between the two resolutions is encouraging, indicating that the current SG setup correctly distributes the fuel-air mixture among the LEM lines, as per the LES solution. Notably, the super-grid resolves the shear layer between the central jet and Slot 1.

Figure 6c, d presents LES results at both resolutions for temperature and CO mass fraction, respectively. The LES temperature results from mapping closure followed by the temperature iteration procedure discussed previously, whereas the LEM-level \tilde{T}_{LEM} purely represents advancement of the LEM domains and the effect of large-scale transport. The LEM-level field is qualitatively similar to the LES field, although of course at a coarser

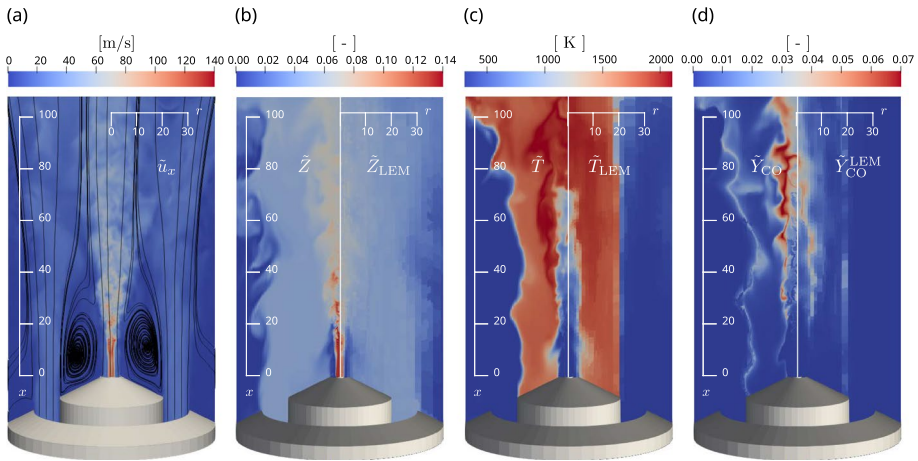


Fig. 6 Instantaneous **a** velocity, **b** mixture fraction, **c** temperature, and **d** CO mass fraction. Streamlines in panel (a) computed with time averaged velocity. Panels (b), (c) and **d** at LES resolution (left half), and at SG resolution (right half) showing LEM-level fields

resolution. Notably, the approach presented in this work is able to reconstruct structures at LES resolution from the coarse-grained distribution of LEM domains. Similarities are also observed for the LES and LEM-level CO mass fractions in Fig. 6d, with high CO levels observed for the inner and outer flame brushes. Slight blocky artefacts are present in the LES CO results, similar to those reported by Menon et al. (2024). These are attributed to the sharply varying levels of intermediate species CO, both spatially and in combined Z - c -space, between adjacent clusters due to the time-scales involved in CO production.

6.2 Radial Profiles

While the similarities in instantaneous structures between the LES and LEM levels are encouraging, the assertion that SG-LEM provides *locally relevant* closure data for LES can be made if there is a similarity in the *mean* (time-averaged) profiles of temperature and composition between the two levels. This would indicate that the mean flame brushes at the LES and LEM levels exhibit a degree of adjacency; hence, the binned data generated by LEM domains in each cluster is locally relevant to the LES-resolved flame. In this section, we perform such a comparison, and also with experimental data using mean and root-mean-square (RMS) profiles for velocity, mixture fraction, temperature, and CO levels. Radial profiles for mean velocity are shown in Figs. 7 (top row) at four axial positions. Near-field values are well captured both for the jet and Slot 2. LES appears to capture the jet breakup in the inner shear layer ($2 \text{ mm} \leq r < 10 \text{ mm}$). Further downstream at $x = 30 \text{ mm}$ and 60 mm , however, centreline velocities are slightly under-predicted and also show greater radial spread. Negative axial velocities show the region of recirculating burnt gases from Slot 2. Similar observations are made for RMS values in Fig. 8 (top row) with better agreement in the near-field, however higher fluctuations in the shear layer are observed here. The mean radial velocity (second row, Fig. 7) also shows good agreement near the burner with a slight over-prediction for Slot 2. At 15 mm , there is a small but noteworthy increase in radial velocity near Slot 1 which indicates a net outward movement of fluid despite recirculation near the region.

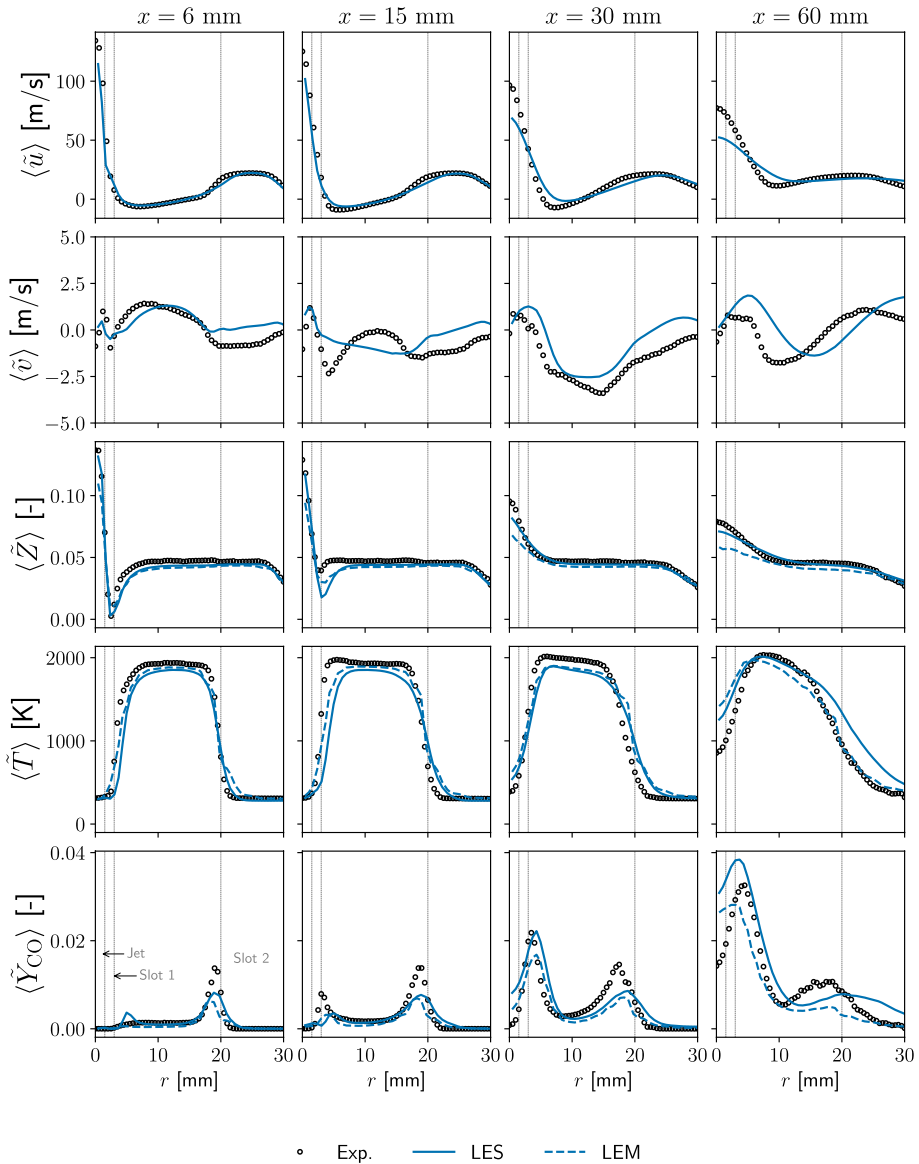


Fig. 7 Time averaged velocity, mixture fraction, temperature and CO mass fraction

Mean mixture fraction in Fig. 7 (third row) show good agreement with experimental data; however, near-field profiles, particularly at 15 mm indicate greater mixing between Slot 1 and hot products from the outer flame, this is observed for both LES and LEM-level values (secondary output) as leaner \tilde{Z} or \tilde{Z}_{LEM} . This correlates with the observed deviation in radial velocity described above. Mixing between the jet and Slot 1 slightly over-predicted at 30 and 60 mm, also indicating a higher radial transport of the jet fluid than seen in the experimental data. RMS profiles are shown in Fig. 8 (second row)

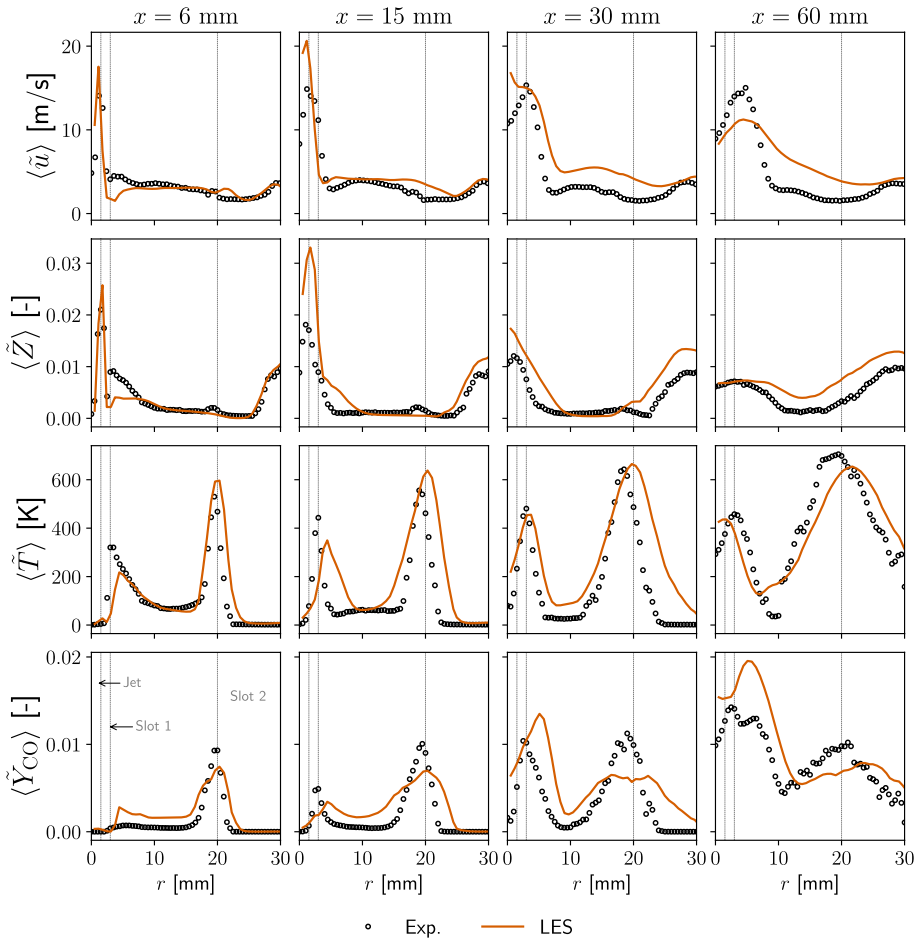


Fig. 8 RMS velocity, mixture fraction, temperature and CO mass fraction

where LES exhibits higher fluctuations in the shear layer between the jet and Slot 1, notably at $x = 15$ mm.

Mean temperature profiles are shown in Fig. 7 (fourth row). Profiles exhibit good agreement with experimental data overall. However, near-field values near the inner shear layer are slightly under-predicted, consistent with leaner mixture fractions. Additionally, LES and splicing transport result in slightly greater radial spread in the far field, this is also likely related to the disparity in radial flux.

Figure 7 (last row) presents mean CO profiles, where the two flame brushes are clearly observed. LES and LEM profiles follow a similar trends except at 6 mm where the presumed PDF mapping shows a slight peak near the inner flame compared the LEM domains. CO levels are correctly captured for the inner flame at $x = 30$ and 60 mm. However a clear under-production is observed for the outer premixed flame for all axial locations. Importantly, this under-production appears to originate from the LEM domains near Slot 2.

Overall, the similarities in mean LES and LEM profiles for mixture fraction, temperature and CO show that flame geometry is qualitatively represented at the super-grid level,

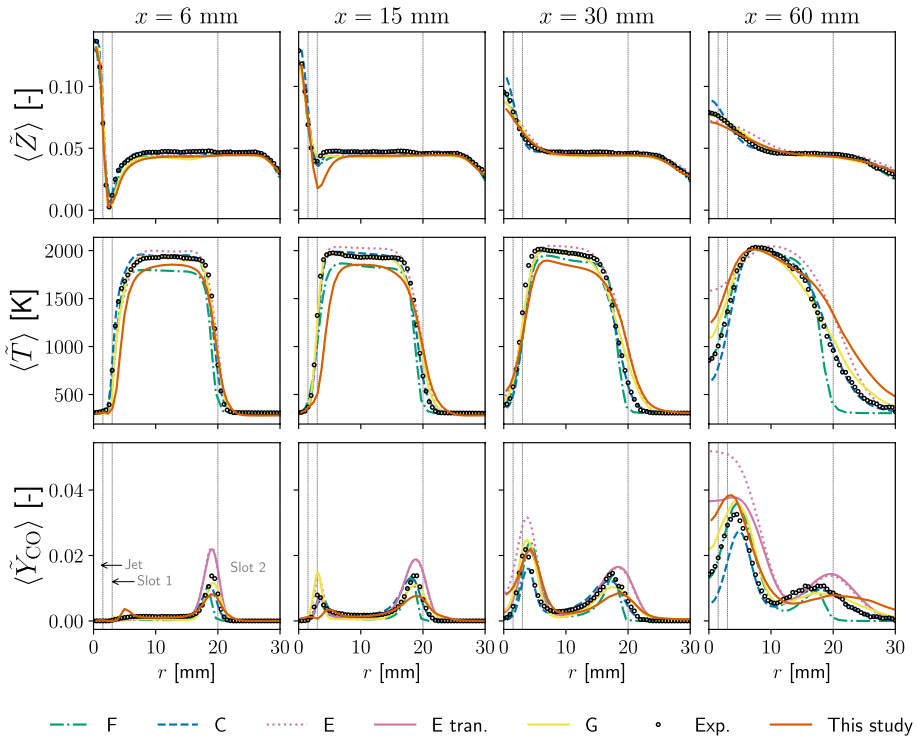


Fig. 9 Comparing SG-LEM with established models; simulation data from Fiorina et al. (2023), cf. Table 1 for parameters

and that the two flame brushes are roughly coincident at the two resolutions. This supports the potential of the (LEM derived) solution tables to be locally relevant for each part of this complex flame case.

6.3 Comparison with Established Models

To better understand the behaviour of the current SG-LEM framework, it is useful to compare it with existing studies using standard well established combustion models. Figure 9 shows the mean scalars (mixture fraction, temperature and CO levels) from a selection of simulations – part of the joint numerical study reported by Fiorina et al. (2023) that involved multiple research groups with disparate simulation strategies. Simulations ‘C’, ‘E’, ‘F’ and ‘G’ are named according to the same reference, parameters for which are listed in Table 1. All simulations were performed using OpenFOAM, employ second-order spatial and temporal schemes, and use a structured LES mesh. C and F use reactor models, i.e., Partially-Stirred Reactor (PaSR) (Chomiak 1990) and Eddy Dissipation Concept (EDC) (Ertesvåg and Magnussen 2000), respectively. Sims. E and G, however, use mapping closures based on tabulated flamelets. Flamelets for E were computed for a freely-propagating configuration whereas Sim. G used a counter-flow configuration. To incorporate TCI, Sim. E utilises the Thickened Flame approach (Colin et al. 2000) in conjunction with a Flame Wrinkling model (Charlette et al. 2002), whereas Sim. G uses a presumed PDF approach. Sim. E also employs a transport equation for

Table 1 Referenced simulations

Sim	Solver	Mesh size (n)	Kinetics	Combustion model
F	low Mach	1 M	17-species skeletal ^a	PaSR
C	compressible	8 M	15-species ARC ^b	EDC
E	low Mach	31 M	GRI-30 ^c	PF, FGM, ATF, FWM
G	low Mach	3.8M	GRI-30	NPF, FPV, presumed PDF

PaSR, Partially-stirred Reactor; PF, Premixed Flamelets; ATF, Artificially Thickened Flames; FWM, Flame Wrinkling Model; ARC, Analytically Reduced Chemistry; EDC, Eddy Dissipation Concept; NPF, Non-premixed Flamelets

^aSame as this study

^bGargiulo et al. (2019)

^cSmith et al.

CO (marked as ‘E tran.’ in the figure) using a mapped source term as an alternate to the mapped CO mass fractions.

SG-LEM results are within the range of comparative simulations using the standard models and can be said to be representative of the MRB flame; however, some important differences can be observed. The excessive mixing at $x = 15\text{mm}$ (first row) is not observed in the referenced cases. While this may explain the lower temperature and CO levels near Slot 1, it is not present in F which uses a coarser LES mesh. A likely source of this error, then, is the time-resolved velocity data used for the jet inflow that was obtained from a precursor LES simulation. Excessive fluctuations in velocity (cf. Fig. 8) could have led to increased turbulent transport of fluid in the radial direction, also seen in Fig. 7. This would also explain the greater fluctuations in \tilde{Z} , as well as the radial spread of \tilde{u} seen for the downstream axial locations.

When comparing the outer flame profiles, SG-LEM appears to produce the least CO. A surprising result here is that Sim. E over-predicts CO, especially near the burner, despite employing a premixed flamelet tabulation. Fiorina et al. (2023) discuss this issue related to flame thickening used in E to resolve the flame front given the employed radial mesh, like the one used in this study. The more accurate, and counter-intuitive, results of Sim. G (using non-premixed flamelets) were explained as resulting from the use of both steady and unsteady flamelets, combined with the non-use of flame thickening. Sim. G shows slight under-production of CO as well and uses a presumed-PDF approach like in this study, although it’s difficult to make an exact comparison as it uses detailed reaction kinetics.

Comparison with Sim. F is of interest here as it uses the same kinetics as this study and even produces similar temperature profiles, except at $x = 60\text{mm}$ due to its coarser resolution. It shows acceptable levels of CO production for the outer flame which implies that the skeletal chemistry used is likely not the source of the CO under-production seen for SG-LEM.

For the inner, multi-regime flame, SG-LEM produces acceptable temperature and CO levels except for $x = 15\text{mm}$ due to the excess mixing mentioned above. All the referenced simulations show some dispersion around the experimental mean values but generally capture the correct trend. As expected, mapping closure using premixed flamelets (E) produces inaccurate CO levels in this region, whereas the CO transport equation (E tran.) shows much better agreement but appears to show early liftoff.

Table 2 Normalized computational time, data for simulations C, E, F and G as reported by Fiorina et al. (2023)

Sim	Core hours (T) 10^3 h	Sim. time (t) s	Comp. time ($T/t/n$)
C	800	0.54	666
F	72	0.4	648
This study	30	0.06	580
E	244	0.08	354
G	9.7	0.04	226

The discussion above briefly touches upon the numerical challenges faced by standard combustion models for this complex case. It should be noted that a fine-grained comparison may not be possible here due to the differing meshing and inflow strategies, nonetheless the referenced simulations help contextualise the model performance of SG-LEM given the state-of-the-art. Table 2 lists normalized computational demand for the referenced simulations as reported by Fiorina et al. (2023). While it was not feasible to conduct a full LES-LEM for this case to estimate the speed-up offered by SG-LEM, the metric used in the above table shows that SG-LEM (for the current setup) is less demanding than the reactor models (F and C) but more than the tabulated chemistry models (E and G).

6.4 Conditional CO Statistics

Conditional statistics can provide more insight into the model performance independent of LES transport inaccuracies related to \tilde{u} , \tilde{Z} and \tilde{c} .

6.4.1 Inner Flame

Figure 10 shows instantaneous scatter plots of CO mass fractions in the Z - Y_C plane for the inner flame, defined as $r \leq 10$ mm. Simulation data for each axial location were obtained within 5 mm slabs centred at each x coordinate shown in the figure. Both LES and LEM data are shown. Note that LES \tilde{Y}_{CO} is plotted against LES \tilde{Z} and \tilde{Y}_C , whereas LEM-level \tilde{Y}_{CO}^{LEM} is plotted against their LEM counterparts. Also included are experimental images from Popp et al. (2021) for direct comparison. SG-LEM accurately reproduces the overall behaviour of the inner flame at the three axial locations. Some notable observations:

- At $x = 15$ mm, both LES and LEM capture the mixing between the burnt products from Slot 2 ($Z = 0.044$) and fresh air from Slot 1 ($Z = 0$), as indicated by trajectory c in the left column. Pure mixing between the jet ($Z = 0.13$) and Slot 1, shown by trajectory a , is also captured. However, the LEM (super-grid) level fails to resolve the lean side completely. The partially premixed region emanating from the jet can be seen as the area between trajectories a and b_r , with b_r representing the rich limit for mixing between the jet and Slot 1. A reaction zone has been established, as seen by the spread in Y_C , supported by the lean premixed flame from Slot 2.
- At $x = 30$ mm, trajectories b_r and b_l represent the rich and lean mixing limits, respectively. As before, LEM resolves a smaller spread in mixture fraction. LES exhibits higher CO levels near the rich limit, which are not seen in the experimental data, while

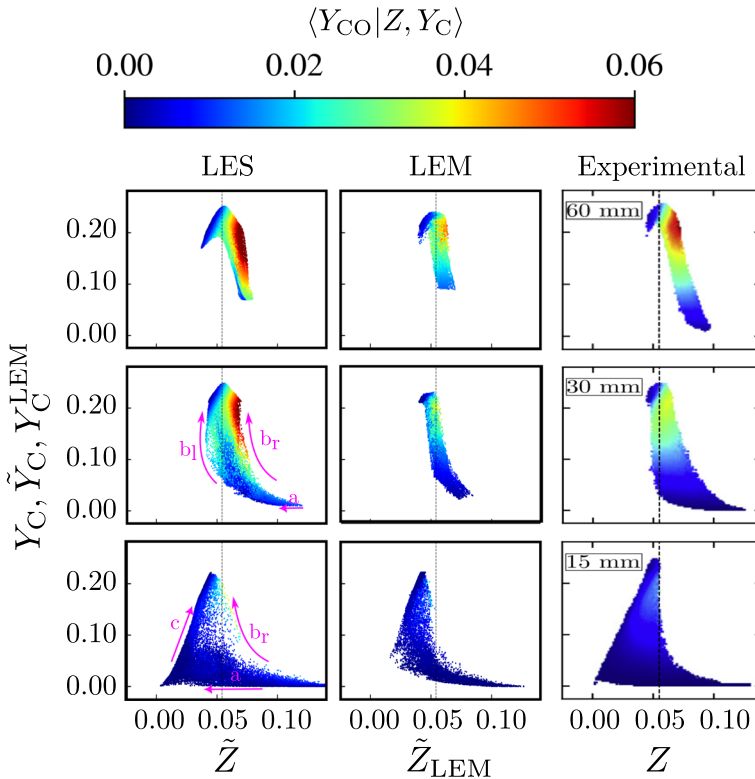


Fig. 10 Conditional CO statistics of inner flame using LES data (left column), LEM-level data (middle column) and experimental images (right column) from Popp et al. (2021) with permission from Elsevier. Rows correspond to streamwise locations indicated in the right column. Dotted lines shows stoichiometric mixture fraction of 0.055

LEM exhibits lower, more accurate, levels. This is somewhat reflected in the mean profiles shown in Fig. 7.

- At $x = 60$ mm, the rich and lean mixing trajectories move closer together, resembling a non-premixed flame but still mixing with burnt products from the outer flame. LES again exhibits higher CO levels than experiment, while LEM exhibits lower levels, also reflected in the mean profiles in Fig. 7. These two resolutions show similar features but do not capture the full range of the experimental data, specifically the unburnt side of rich mixtures.

The above is indicative of SG-LEM’s ability to represent the general topology of the inner flame, despite inaccuracies in the radial flux. The phenomenon of flame lift-off³ requires LEM domains to accurately capture mixing between the jet and Slot 1 so that the correct regions fall in the flammability limit, simulate entrainment of hot gases from Slot 2, and finally, simulate the turbulent flame speed in the hot environment.

³ Note that there is no exact lift-off length provided in Butz et al. (2022)

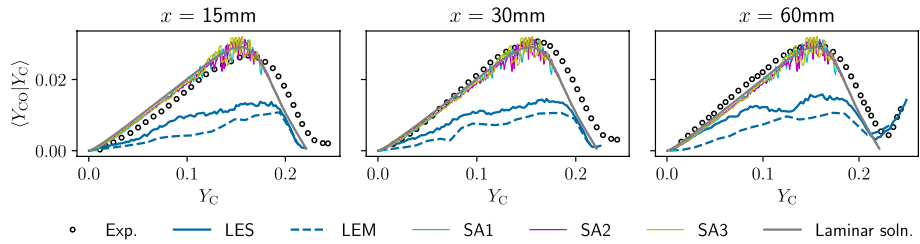


Fig. 11 Conditional CO statistics for the outer flame. Laminar profile and stand-alone LEM simulations (SA1-3) using $Z = 0.044$ shown for comparison. SA1: $Re_t = 100$; SA2: $Re_t = 50$; SA3: $Re_t = 50$, time-accurate eddy implementation

6.4.2 Outer Flame

Figure 11 shows CO conditionally averaged on Y_C for the outer flame, defined as $r > 10$ mm. It clearly shows under-production of CO. The laminar flame profile in the figure represents the initial value of all solution tables in the domain (for the bin near $Z = 0.044$); hence, the lower values represent LEM domain states. At $x = 60$ mm, LEM and LES profiles exhibit a final burst of reaction for $Y_C > 0.21$, before reactant depletion. This is seen for the experimental data at a higher Y_C value (≈ 0.23).

To determine the origin of the CO under-production, which was not observed in the previous application (Menon et al. 2024), stand-alone LEM simulations of a freely propagating flame subject to triplet-map stirring (at $Z = 0.044$) were conducted for comparison. The domains were 5 mm in length, roughly the cluster domain size near the outer flame, and subject to $Re_t = 100$ and 50, which broadly captures the range observed near the outer flame as given by Eq. (30). The flame region was continually maintained in the middle of the domain via splicing of fresh charge and burnt products which allowed for conditional averaging of scalars, over time, using the same procedure as SG-LEM. These are given by ‘SA[1-3]’ in the figure, and show that the stand-alone LEM simulations cannot not reproduce the low CO levels despite replicating (LEM) conditions near Slot 2. This indicates that the source of this error is not LEM advancement per se. A comparison of the time-accurate eddy implementation (SA 3) with the blocked-sequence eddy-implementation (SA 2) showed only subtle differences, i.e. the splitting bias introduced by the blocked approach is also not sufficient to cause this issue.⁴ The similarity in LEM and LES profiles also rules out the presumed-PDF mapping as being the major error source. Mean temperature and mixture fraction are also correctly predicted at both resolutions.

The above process of elimination narrows down the source of CO under-production to mass exchange between LEM domains, which consists of large-scale splicing and the lack of inter-cluster (inter-LEM) diffusion in the current framework. The second factor is of import near Slot 2 as the flow is parallel to the boundary between burnt and unburnt clusters. LEM domains can only exchange mass through splicing, which is driven by low face-normal fluxes in the region. Traditional LES-LEM, which is tailored to high- Re cases, assumes that turbulent mixing greatly exceeds molecular mixing. Thus, resolved (and

⁴ Time-accurate eddy implementation also required around 7 times the simulation time (for $Re_t = 50$) than the blocked-sequence approach when using time-steps similar to LES (5×10^{-7} s). This justifies the use of the latter approach without much loss in accuracy.

optionally SGS) fluxes that drive splicing transport can compensate for the lack of inter-LEM diffusion, an approach which is problematic near the laminar flame limit. The use of a coarse-grained mesh in SG-LEM accentuates this issue as LES-resolved fluxes are summed over cluster boundaries for splicing, thus effectively smoothing out the resolved turbulence which might have otherwise compensated for the lack of inter-cluster diffusion. In other words, SG-LEM may not accurately represent a premixed flame structure in this outer region, despite the proven ability of stand-alone LEM to do the same. Nonetheless, a high temperature region is established near Slot 2 which provides a reservoir of burnt LEM fragments that support the support the inner flame by splicing entrainment. Evidently, the lack of inter-LEM diffusion is not detrimental to the inner flame simulation, this is likely due to the high velocities and shear turbulence caused by the jet, as well as the much smaller cluster dimensions due to the radial nature of the LES mesh.

7 Conclusion and Future Work

Super-grid LEM (SG-LEM) is a method developed to overcome the major drawback of LES-LEM, i.e., simulation time, while retaining the benefits of LEM modelling. This is achieved using LES mesh agglomeration and utilises chemistry tabulation alongside the presumed PDF approach to mapping closure to reconstruct LES-resolved scalars. The method uses a modified LES-LEM ‘splicing’ scheme to simulate large-scale advective transport between LEM domains. It was first validated for a premixed ethylene-air DNS case and was shown to accurately predict scalar fields including CO. The present work investigates the performance of SG-LEM for a challenging multi-regime scenario which exhibits premixed and non-premixed attributes – the Darmstadt Multi-Regime Burner (MRB).

SG-LEM simulation of the MRB case showed strong sensitivity to the clustering parameters used to generate the super-grid (SG), in particular affecting flame stability. The solution involved the use of flow-aligned agglomerations (clusters) that were generated by constraining the `MGRIDGEN` clustering routine using a structured processor decomposition, which led to a stable flame. Instantaneous fields show how the flame topology is qualitatively captured at both LES and SG resolutions, including the premixed outer flame, multi-regime inner flame, lift-off of the inner flame, and the recirculating fluid downstream of the burner. Radial profiles (mean and RMS) for velocity, mixture fraction, temperature and CO mass fraction were compared to experimental data using as well as standard combustion models: premixed/non-premixed flamelets, PaSR and EDC. SG-LEM is broadly representative of the MRB flame, except for under-production of CO near the outer (premixed) flame despite good temperature prediction. Conditional statistics were used to demonstrate that the model can represent mixing trajectories and CO production for the inner, multi-regime, flame. Conditional statistics were also used to investigate the CO under-production for the outer premixed flame, as were stand-alone LEM simulations to replicate cluster LEM conditions near the problematic region. Results strongly indicate that the issue stems from inaccuracies in mass exchange between LEM domains in the region, in particular due to a lack of inter-cluster diffusion.

In conclusion, the study demonstrates the ability of the still-evolving SG-LEM model to handle complex multi-regime scenarios. Crucially, it identifies two areas of improvement for the current framework: 1. cluster generation that does not destroy flame geometry; and 2. a need to model (or compensate for the lack of) inter-cluster/LEM diffusion in regions

where the splicing flux is parallel to cluster boundaries. While these are not strictly related to multi-regime combustion, it would direct SG-LEM towards being a more general-purpose combustion model.

The first issue is related to splicing transport, which was tackled in this study using an indirect approach that involved processor decomposition. This may not be suitable for complex geometries and may not be ideal for load-balancing. In theory, smaller cluster sizes should reduce splicing inaccuracies, but has the disadvantage of proportionately larger compute times. Hence, a super-grid sensitivity study is required for the MRB case. The following pathways are being considered for future implementations of SG-LEM: a more sophisticated splicing scheme that takes cluster geometry into account and can more accurately represent fluid residence times on LEM domains w.r.t. LES. If implemented, automated clustering can be used as in this study. Alternatively, a composite/overset super-grid can be constructed based on physical criteria, as opposed to the physics-agnostic mesh agglomeration used in the current framework, in this case the current splicing scheme can be used unmodified.

As for the second issue, a ‘cross-term’, as discussed in Sec. 10.6.2 of Menon and Kerstein (2011), can be incorporated in future SG-LEM implementations to increase the interaction between burnt and unburnt LEM domains in the specific scenario.

Acknowledgements The authors are grateful to Christian Hasse and Vinzenz Schuh at Simulation reaktiver Thermo-Fluid Systeme (STFS), TU Darmstadt for providing the mesh and useful discussions; we thank Andreas Dreizler at Reactive Flows and Diagnostics, TU Darmstadt, for providing the experimental data; and finally, we thank Benoît Fiorina and Tan-Phong Luu at Laboratoire EM2C, Université Paris-Saclay, for providing the data for the referenced simulations. Computations were performed at the Chalmers Centre for Computational Science and Engineering (C3SE), part of the Swedish National Infrastructure for Computing (SNIC) through projects SNIC 2019/3-181, 2020/6-187, 2020/5-200 and 2022/23-413.

Funding Open access funding provided by Chalmers University of Technology. The work was partially funded by the Swedish Research Council through grant agreement no. 2018-05973.

Declarations

Conflict of interest The authors have no Conflict of interest to disclose.

Open Access This article is licensed under a Creative Commons Attribution 4.0 International License, which permits use, sharing, adaptation, distribution and reproduction in any medium or format, as long as you give appropriate credit to the original author(s) and the source, provide a link to the Creative Commons licence, and indicate if changes were made. The images or other third party material in this article are included in the article’s Creative Commons licence, unless indicated otherwise in a credit line to the material. If material is not included in the article’s Creative Commons licence and your intended use is not permitted by statutory regulation or exceeds the permitted use, you will need to obtain permission directly from the copyright holder. To view a copy of this licence, visit <http://creativecommons.org/licenses/by/4.0/>.

References

- Arshad, S., Kong, B., Kerstein, A.R., Oevermann, M.: A strategy for large-scale scalar advection in large eddy simulations that use the linear eddy sub-grid mixing model. *Int. J. Numer. Methods Heat Fluid Flow* **28**(10), 2463–2479 (2018)
- Arshad, S.: Large eddy simulation of combustion using linear-eddy subgrid modeling. PhD thesis, Chalmers University of Technology, Göteborg, Sweden (2019)
- Bilger, R.W.: Reaction rates in diffusion flames. *Combust. Flame* **30**, 277–284 (1977)
- Butz, D., Breicher, A., Barlow, R.S., Geyer, D., Dreizler, A.: Turbulent multi-regime methane-air flames analysed by Raman/Rayleigh spectroscopy and conditional velocity field measurements. *Combust. Flame* **243**, 111941 (2022)

- Butz, D., Hartl, S., Popp, S., Walther, S., Barlow, R.S., Hasse, C., Dreizler, A., Geyer, D.: Local flame structure analysis in turbulent CH₄/air flames with multi-regime characteristics. *Combust. Flame* **210**, 426–438 (2019)
- Calhoon, W.H., Menon, S.: Subgrid Modeling for Reacting Large Eddy Simulations. In: 34th Aerospace Sciences Meeting and Exhibit. American Institute of Aeronautics and Astronautics, Reno (1996)
- Charlette, F., Meneveau, C., Veynante, D.: A power-law flame wrinkling model for LES of premixed turbulent combustion Part I: Non-dynamic formulation and initial tests. *Combust. Flame* **131**(1), 159–180 (2002)
- Chomiak, J.: *Combustion a Study in Theory Fact and Application*. Abacus Press, Philadelphia (1990)
- Colin, O., Ducros, F., Veynante, D., Poinso, T.: A thickened flame model for large eddy simulations of turbulent premixed combustion. *Phys. Fluids* **12**(7), 1843–1863 (2000)
- Darbyshire, O.R., Swaminathan, N.: A presumed joint pdf model for turbulent combustion with varying equivalence ratio. *Combust. Sci. Technol.* **184**(12), 2036–2067 (2012)
- Doubiani, N., Kerstein, A.R., Oevermann, M.: a pressure-coupled representative interactive linear eddy model (RILEM) for engine simulations. *Fuel* **355**, 129423 (2024)
- Engelmann, L., Wollny, P., Breicher, A., Geyer, D., Chakraborty, N., Kempf, A.: Numerical analysis of multi-regime combustion using flamelet generated manifolds - a highly-resolved Large-Eddy Simulation of the Darmstadt multi-regime burner. *Combust. Flame* **251**, 112718 (2023)
- Ertesvåg, I.S., Magnussen, B.F.: The eddy dissipation turbulence energy cascade model. *Combust. Sci. Technol.* **159**(1), 213–235 (2000)
- Fiorina, B., Luu, T.P., Dillon, S., Mercier, R., Wang, P., Angelilli, L., Ciottoli, P.P., Hernández-Pérez, F.E., Valorani, M., Im, H.G., Massey, J.C., Li, Z., Chen, Z.X., Swaminathan, N., Popp, S., Hartl, S., Nicolai, H., Hasse, C., Dreizler, A., Butz, D., Geyer, D., Breicher, A., Zhang, K., Duwig, C., Zhang, W., Han, W., van Oijen, J., Péquin, A., Parente, A., Engelmann, L., Kempf, A., Hansinger, M., Pfitzner, M., Barlow, R.S.: A joint numerical study of multi-regime turbulent combustion. *Appl. Energy Combust. Sci.* **16**, 100221 (2023)
- Floyd, J., Kempf, A.M., Kronenburg, A., Ram, R.H.: A simple model for the filtered density function for passive scalar combustion LES. *Combust. Theory Model.* **13**(4), 559–588 (2009)
- Gargiulo, G., Ciottoli, P.P., Martelli, E., Malpica Galassi, R., Valorani, M.: Numerical analysis of laser-pulse transient ignition of oxygen/methane mixtures in rocket-like combustion chamber. *Acta Astronaut.* **159**, 136–155 (2019)
- Grøvdal, F.: A dimensional-decomposition approach for stochastic scale-resolving simulations of turbulent reacting flows. Doctoral thesis, NTNU (2018)
- Hindmarsh, A.C., Brown, P.N., Grant, K.E., Lee, S.L., Serban, R., Shumaker, D.E., Woodward, C.S.: SUNDIALS: Suite of Nonlinear and Differential/Algebraic Equation Solvers. *ACM Trans. Math. Softw.* **31**(3), 363–396 (2005)
- Issa, R.I., Gosman, A.D., Watkins, A.P.: The computation of compressible and incompressible recirculating flows by a non-iterative implicit scheme. *J. Comput. Phys.* **62**(1), 66–82 (1986)
- Jasak, H.: Error analysis and estimation for the finite volume method with applications to fluid flows. PhD thesis, Imperial College of Science, Technology and Medicine (June 1996)
- Kerstein, A.R.: Linear-eddy modelling of turbulent transport. part 6. microstructure of diffusive scalar mixing fields. *J. Fluid Mech.* **231**, 361–394 (1991)
- Kerstein, A.R., Cremer, M.A., McMurtry, P.A.: Scaling properties of differential molecular diffusion effects in turbulence. *Phys. Fluids* **7**(8), 1999–2007 (1995)
- Lackmann, T., Kerstein, A.R., Oevermann, M.: A representative Linear Eddy Model for simulating spray combustion in engines (RILEM). *Combust. Flame* **193**, 1–15 (2018)
- Li, S., Li, S., Mira, D., Zhu, M., Jiang, X.: Investigation of dilution effects on partially premixed swirling syngas flames using a LES-LEM approach. *J. Energy Inst.* **91**(6), 902–915 (2018)
- Li, S., Zheng, Y., Mira, D., Li, S., Zhu, M., Jiang, X.: A Large-Eddy Simulation-Linear-Eddy Model Study of Preferential Diffusion Processes in a Partially Premixed Swirling Combustor With Synthesis Gases. *J. Eng. Gas Turbines Power* **139**, 031501 (2016)
- Maxwell, B.M., Falle, S.A.E.G., Sharpe, G., Radulescu, M.I.: A compressible-LEM turbulent combustion subgrid model for assessing gaseous explosion hazards. *J. Loss Prev. Process Ind.* **36**, 460–470 (2015)
- McBride, B.J., Zehle, M.J., Gordon, S.: NASA glenn coefficients for calculating thermodynamic properties of individual species. Technical report (2002)
- Menon, S., Calhoon, W.H.: Subgrid mixing and molecular transport modeling in a reacting shear layer. *Symp. (Int.) Combust.* **26**(1), 59–66 (1996)
- Menon, A.M., Oevermann, M., Kerstein, A.R.: A super-grid approach for LES combustion closure using the Linear Eddy Model. *Combust. Theor. Model.* **28**(1), 99–126 (2024)

- Menon, S., Kerstein, A.R.: The linear-Eddy Model. In: Turbulent Combustion Modeling: Advances, New Trends and Perspectives, pp. 221–247. Springer, (2011)
- Moulitsas, I., Karypis, G.: Serial/Parallel Library for Generating Coarse Grids for Multigrid Methods. Technical report (May 2001)
- Pellegrini, F., Roman, J.: Scotch: A software package for static mapping by dual recursive bipartitioning of process and architecture graphs. In: Liddell, H., Colbrook, A., Hertzberger, B., Sloot, P. (eds.) High-Performance Computing and Networking, pp. 493–498. Springer, Berlin, Heidelberg (1996)
- Pierce, C.D., Moin, P.: A dynamic model for subgrid-scale variance and dissipation rate of a conserved scalar. *Phys. Fluids* **10**(12), 3041–3044 (1998)
- Popp, S., Hartl, S., Butz, D., Geyer, D., Dreizler, A., Vervisch, L., Hasse, C.: Assessing multi-regime combustion in a novel burner configuration with Large Eddy simulations using tabulated chemistry. *Proc. Combust. Inst.* **38**(2), 2551–2558 (2021)
- Ranjan, R., Muralidharan, B., Nagaoka, Y., Menon, S.: Subgrid-Scale modeling of reaction-diffusion and scalar transport in turbulent premixed flames. *Combust. Sci. Technol.* **188**(9), 1496–1537 (2016)
- Sankaran, R., Hawkes, E.R., Chen, J.H., Lu, T., Law, C.K.: Structure of a spatially developing turbulent lean methane-air bunsen flame. *Proc. Combust. Inst.* **31**(1), 1291–1298 (2007)
- Sankaran, V.: Sub-grid Combustion Modeling for Compressible Two-Phase Flows. PhD thesis, Georgia Institute of Technology (November 2003)
- Smagorinsky, J.: General circulation experiments with the primitive equations: I. The basic experiment. *Mon. Weather Rev.* **91**(3), 99–164 (1963)
- Smith, T.M., Menon, S.: One-dimensional simulations of freely propagating turbulent premixed flames. *Combust. Sci. Technol.* **128**(1–6), 99–130 (1997)
- Smith, G.P., Golden, D.M., Frenklach, M., Moriarty, N.W., Eiteneer, B., Goldenberg, M., Bowman, C.T., Hanson, R.K., Song, S., Gardiner, W.C. Jr., Lissianski, V.V., Qin, Z.: GRI-Mech 3.0. http://www.me.berkeley.edu/gri_mech/
- Smith, T.M., Menon, S.: Subgrid Combustion Modeling for Premixed Turbulent Reacting Flows. In: 36th AIAA Aerospace Sciences Meeting and Exhibit. American Institute of Aeronautics and Astronautics, Reno, NV, U.S.A. (1998)
- Sutherland, W.: LII The viscosity of gases and molecular force. *Lond. Edinb. Dublin Philos. Mag. J. Sci.* **36**(223), 507–531 (1893)
- Zhang, W., Han, W., Wang, J., Huang, Z., Jin, W., van Oijen, J.: Large-eddy simulation of the Darmstadt multi-regime turbulent flame using flamelet-generated manifolds. *Combust. Flame* **257**, 113001 (2023)

Publisher's Note Springer Nature remains neutral with regard to jurisdictional claims in published maps and institutional affiliations.

Authors and Affiliations

Abhilash Menon¹ · Alan Kerstein² · Michael Oevermann^{1,3}

✉ Abhilash Menon
menona@chalmers.se

Alan Kerstein
alan.kerstein@gmail.com

Michael Oevermann
michael.oevermann@b-tu.de

¹ Mechanics and Maritime Sciences, Chalmers Tekniska Högskola, 41258 Gothenburg, Sweden

² Danville, USA

³ Department of Numerical Mathematics and Scientific Computing, Brandenburgische Technische Universität, 03046 Cottbus, Germany